IEEE Access
Multidisciplinary | Rapid Review | Open Access Journal

Received May 20, 2018, accepted June 19, 2018, date of publication June 26, 2018, date of current version July 12, 2018.

Digital Object Identifier 10.1109/ACCESS.2018.2850758

Hybrid-Level Joint-Drift-Free Scheme of Redundant Robot Manipulators Synthesized by a Varying-Parameter Recurrent Neural Network

ZHIJUN ZHANG, (Member, IEEE), AND ZIYI YAN
School of Automation Science and Engineering, South China University of Technology, Guangzhou 510641, China
Corresponding author: Zhijun Zhang (drzhangzhijun@gmail.com)

This work was supported in part by the National Key R&D Program of China under Grant 2017YFB1002505, in part by the National Natural Science Foundation of China under Grant 61603142 and Grant 61633010, in part by the Guangdong Foundation for Distinguished Young Scholars under Grant 2017A030306009, in part by the Guangdong Youth Talent Support Program of Scientific and Technological Innovation under Grant 2017TQ04X475, in part by the Science and Technology Program of Guangzhou under Grant 201707010225, in part by the Fundamental Research Funds for Central Universities under Grant 2017MS049, in part by the Scientific Research Starting Foundation of South China University of Technology, in part by the National Key Basic Research Program of China (973 Program) under Grant 2015CB351703, and in part by the Natural Science Foundation of Guangdong Province under Grant 2014A030312005.

ABSTRACT For a redundant robot manipulator, the external perturbation and digital computation errors are inevitable when executing a tracking task. In this paper, a hybrid-level joint-drift-free (HL-JDF) scheme is proposed and synthesized by a novel varying-parameter recurrent neural network [called varying-parameter convergent-differential neural network (VP-CDNN)] with inherent perturbation tolerance. The HL-JDF scheme is combined with torque and velocity level optimization schemes and aims to solve the joint-drift problem with noise considered in the tracking task of redundant robot manipulators. The tracking task of a redundant robot manipulator is first formulated as a time-varying convex quadratic programming (QP) problem. Second, the QP problem is converted into a matrix equation. Finally, the proposed VP-CDNN is applied to solve the matrix equation. What is more, theoretical robustness analysis of the proposed VP-CDNN is presented. In addition, computer simulations and physical experiments of a redundant robot tracking task synthesized by the proposed VP-CDNN and the conventional fixed-parameter convergent-differential neural network (FP-CDNN) are conducted for illustrations and comparisons. Both the theoretical analysis and experiment results prove the effectiveness of the proposed HL-JDF scheme and the higher accuracy and better ability to resist the disturbance of the proposed VP-CDNN compared with the traditional FP-CDNN.

INDEX TERMS Robotics, recurrent neural networks, quadratic programming, robustness.

I. INTRODUCTION

In recent years, robots have developed rapidly and are widely applied in more and more fields [1]–[6]. Robotic researches are working to utilize the robots to finish a variety of tasks in sophisticated environments. A robot manipulator is called redundant robot manipulator as its degrees-of-freedom (DOF) are more than the least number of DOF to finish the primary task [3]. A redundant manipulator, while performing a primary task, can also execute additional subtasks such as avoiding obstacles [7], [8], avoiding singular configuration [9], [10], and planning cyclic motion [11], [12].

Joint-drift-free motion (or repetitive motion) means that all the joints of a manipulator should return their initial states when the robot manipulator finishes once closed end-effector tracking task. Joint-drift-free motion is usually a basic requirement in industry production procedures. If the control scheme does not consider the joint-drift-free criterion, a joint-drift phenomenon would happen and result in the different initial states of the manipulator in the cyclic operation. This will lead to the rapid decline in operation accuracy and an extra adjustment is needed. There is no doubt that the production efficiency would be impacted if the joint-drift-free criterion is not considered [11].

A fundamental issue in controlling redundant robot manipulators is the inverse-kinematics problem. There exist multiple feasible solutions to the inverse-kinematics problem of a redundant robot manipulator due to the non-linear and redundancy. The conventional approach to solving the inverse-kinematic is the pseudo-inverse based method [13]. However the conventional pseudo-inverse based method needs to calculate the inverse of a matrix which may cost much more time. Furthermore, the conventional pseudo-inverse based method is difficult to consider the optimization criterions.

In recent years, researches tend to solve the inverse-kinematics problems by using quadratic programming (QP). In this way, the inverse-kinematics of redundant robot manipulators are formulated into a QP constrained by the kinematics and dynamic equations. In order to achieve a more rational distribution of joint-torque, some researches about torque optimization of robot manipulators have been implemented [14]–[17]. A minimum torque norm (MTN) scheme was proposed in [17] to solve the tracking problem of redundant robot manipulators at torque level. Guo *et al.* [14] combined the minimum two-norm joint-velocity and infinity-norm joint-torque schemes to remedy the joint-torque divergence problem. Meanwhile, a scheme which consists of the minimum two-norm joint-velocity and joint-torque solutions was proposed to prevent occurrence of high joint-velocity and guaranteed the final joint-velocity to be close to zero [15]. However, the joint-drift-free motion was not considered in these dynamic schemes of redundant robot manipulators. In this paper, a hybrid-level joint-drift-free (HL-JDF) scheme is proposed and investigated to solve the joint-drift problem in the end-effector tracking task of redundant robot manipulators. Meanwhile, the proposed HL-JDF scheme also can prevent high joint-velocity and achieve rational distribution of joint-torque.

Neural network methods are considered as a powerful tool to solve convex QP problems due to the parallel computing methods [11], [17]–[21]. Wang presented a traditional gradient-based neural network for solving QP problems with an equality constraint [22]. However, Wang's method cannot track well the theoretical solutions in limit time. In order to improve the computation performance, Zhang *et al.* [23] proposed a fixed parameter recurrent neural network (Zhang neural network) to solve the time-varying QP problems, which has faster convergence speed and higher accuracy compared with Wang's method.

It is worth pointing out that the differential errors or measurement noises are not considered when the above mentioned neural-dynamic based methods are used to solve QP problems and robot inverse kinematic problems. However, when robot manipulators are executing tasks, the hardware implementation, external disturbances and digital computation errors always exist. The robustness of Zhang's method for solving time-varying convex QP problems with external perturbation and digital computation errors are discussed and analyzed in [24]. From the simulation results of [24], we can see that the residual errors cannot converge to zero. Jin el al. proposed a modified gradient neural network with noise tolerance and applied to redundant robot manipulators [21]. He just considered the measurement noises or perturbation, but did not consider digital computation errors. Different from this inspiring work, in this paper, a novel varying-parameter convergent-differential neural network (VP-CDNN) is proposed with external perturbation and digital computation errors considered. Due to the super exponential convergence speed and strong robustness of the proposed VP-CDNN, it is more efficient to solve the perturbed tracking problems of redundant robot manipulators.

The remainder of this paper is organized as follows. In Section II, the HL-JDF scheme is formulated, and the VP-CDNN is illustrated and exploited to solve the HL-JDF scheme. For comparison analysis, the conventional FP-CDNN is also presented in this section. Then the robustness of the VP-CDNN is analyzed in Section III. Section IV presents simulations and experiments to demonstrate the effectiveness of the proposed HL-JDF scheme and the robustness and accuracy of the proposed VP-CDNN. Section V draws the conclusion. The main contributions of this paper are listed as the following facts.

- A hybrid-level joint-drift-free (HL-JDF) scheme is proposed to solve the joint-drift problem of redundant robot manipulators. Meanwhile, high joint-velocity and joint-torque can be prevented during the tracking task.
- A novel varying-parameter convergent-differential neural network (VP-CDNN) is proposed and exploited to solve the HL-JDF scheme. The theoretical proofs of convergence and robustness of the VP-CDNN is given in detail.
- Simulations and experiments are presented to demonstrate the effectiveness of the HL-JDF scheme and the robustness and accuracy of the VP-CDNN.

II. PROBLEM FORMULATION AND NEURAL NETWORK MODEL

In this section, the preliminaries of redundant robot manipulators' inverse-kinematics are firstly presented. Then the HL-JDF scheme is formulated into a unified QP. Finally, the VP-CDNN is proposed and applied to solve the QP problem. For comparisons and illustrations, the conventional FP-CDNN is also presented in this section.

A. HL-JDF SCHEME FORMULATION

Consider the inverse-kinematics of redundant robot manipulators at the velocity level, i.e.,

$$J(\theta)\dot{\theta}(t) = \dot{r}(t) \tag{2.1}$$

where $J(\theta) \in R^{m\times n}$ is the Jacobian matrix of a robot manipulator; n denotes the number of manipulator joints and m denotes spatial dimension of end-effector position; $\theta(t) \in R^n$ are joint angular vector; $\dot{r}(t) \in R^m$ and $\dot{\theta}(t) \in R^n$ are the end-effector velocity vector and the joint angular velocity vector, respectively.

In order to prevent high joint-velocity and achieve rational distribution of joint-torque, we combine the minimum torque norm (MTN) scheme and minimum velocity norm (MVN) scheme through a weighting coefficient $\zeta \in [0, 1]$, and consider the joint-drift-free criterion and feedback control, then the proposed HL-JDF scheme can be written as

$$\text{minimize } \frac{1}{2}(\zeta\|\dot{\theta}(t)+s(t)\|_2^2+(1-\zeta)\|\tau\|_2^2) \quad (2.2)$$

$$\text{subject to } J\ddot{\theta}(t)=\ddot{r}(t)-\dot{J}\dot{\theta}+\rho_{\mathrm{v}}(\dot{r}(t)-J\dot{\theta}) + \rho_{\mathrm{p}}(r(t)-f(\theta)) \quad (2.3)$$

$$\tau = H(\theta)\ddot{\theta}+c(\theta,\dot{\theta})+g(\theta) \quad (2.4)$$

where $s(t) = \mu(\theta(t) - \theta(0))$ is the joint-drift criterion with $\mu > 0$ denoting the response of joint-drift $\theta(t)-\theta(0)$; ρ_{v} and ρ_{p} are feedback-control coefficients; and τ is the joint-torque vector determined by the dynamic equation (2.4) with $H(\theta) \in R^{n\times n}$ denoting the inertia matrix, $c(\theta, \dot{\theta}) \in R^n$ denoting the Coriolis and centrifugal force vector, and $g(\theta) \in R^n$ denoting the gravitational force vector. It is worth pointing out that the HL-JDF scheme can be simplified as the MTN scheme (when $\zeta = 0$), and the MVN scheme (when $\zeta = 1$). According to the equivalence theorem of different-level scheme [25], $\|\dot{\theta}(t) + s(t)\|_2^2$ is equivalent to $\|\ddot{\theta}(t)+\sigma(t)\|_2^2$ where $\sigma(t) = (\alpha+\beta)\dot{\theta}+\alpha\beta(\theta-\theta(0))$. In order to obtain the unified QP formulation, we consider problems at acceleration level and then HL-JDF scheme (2.2)-(2.4) can be rewritten as

$$\text{minimize } x(t)^{\mathrm{T}}Wx(t)/2+\eta^{\mathrm{T}}(t)x(t) \quad (2.5)$$

$$\text{subject to } Jx(t)=b(t) \quad (2.6)$$

where $x := \ddot{\theta}$, $W := \zeta I + (1-\zeta)H^2$, $\eta := \zeta\sigma(t) + (1-\zeta)H^{\mathrm{T}}(c+g)$, $\sigma(t) = (\alpha+\beta)\dot{\theta}+\alpha\beta(\theta-\theta(0))$, $b(t) := \ddot{r}(t) - \dot{J}\dot{\theta}+\rho_v(\dot{r}-J\dot{\theta})+\rho_p(r-f(\theta))$; I is identity matrix; α, β, ρ_v and ρ_p are positive parameters.

B. NEURAL NETWORK MODEL

In order to solve the QP problems (2.5) and (2.6), according to Lagrange method and neural dynamic design method [19], a novel varying-parameter convergent-differential neural network (VP-CDNN) is proposed. For comparison analysis, the traditional fixed-parameter convergent-differential neural network (FP-CDNN) is also presented in this subsection.

A Lagrange function is firstly formulated from QP problems (2.5) and (2.6), i.e.,

$$L(x(t),\lambda(t),t) = x^{\mathrm{T}}(t)Wx(t)/2+\eta^{\mathrm{T}}(t)x(t) + \lambda^{\mathrm{T}}(t)(J(t)x(t)-b(t)), \quad t\in[0,+\infty) \quad (2.7)$$

where $\lambda(t) \in R^m$ denotes a Lagrange multiplier vector. The partial derivatives of Equation (2.7) are

$$\begin{cases} \dfrac{\partial L(x(t),\lambda(t),t)}{\partial x(t)} = Wx(t)+\eta(t)+J^{\mathrm{T}}(t)\lambda(t)=0, \\ \dfrac{\partial L(x(t),\lambda(t),t)}{\partial \lambda(t)} = J(t)x(t)-b(t)=0. \end{cases}$$

Combining the above two partial derivatives together, we can get the following matrix function,

$$Qy = u \quad (2.8)$$

where

$$Q := \begin{bmatrix} W & J^{\mathrm{T}}(t) \\ J(t) & 0 \end{bmatrix} \in R^{(n+m)\times(n+m)}$$

$$y := \begin{bmatrix} x(t) \\ \lambda(t) \end{bmatrix} \in R^{n+m} \quad u := \begin{bmatrix} -\eta(t) \\ b(t) \end{bmatrix} \in R^{n+m}.$$

According to the above conversion, solving QP problems (2.5) and (2.6) is equivalent to solving the matrix equation (2.8). In order to obtain the solution to matrix equation (2.8), an error function is defined as

$$\varepsilon(t) = Qy - u \in R^{n+m}. \quad (2.9)$$

Since the error $\varepsilon(t)$ is desired to converge to zero, and in order to obtain the super exponential convergence speed of $\varepsilon(t)$, we design a neural dynamic formula as

$$\frac{d\varepsilon(t)}{dt} = -\gamma\exp(t)\Phi(\varepsilon(t)) \quad (2.10)$$

where $\gamma\exp(t)$ is applied to scaling the convergence rate with $\gamma > 0$; $\Phi(\cdot) : R^{n+m} \to R^{n+m}$ denotes an activation-function processing-array.

Finally, substituting Equation (2.9) into Equation (2.10), the following implicit-dynamic equation is obtained, i.e.,

$$Q\dot{y} = -\dot{Q}y-\gamma\exp(t)\Phi(Qy-u)+\dot{u} \quad (2.11)$$

where $\dot{Q} = \mathrm{d}Q/\mathrm{d}t$, $\dot{u} = \mathrm{d}u/\mathrm{d}t$. Since the designed parameter $\gamma\exp(t)$ in Equation (2.10) and (2.11) is time-varying and the design process is based on differential equation theorem, the implicit-dynamic equation (2.11) is termed as varying-parameter convergent-differential neural networks (VP-CDNN).

In order to describe the structure of the proposed VP-CDNN, Equation (2.11) can be rewritten as

$$\dot{y} = (I-Q)\dot{y}-\dot{Q}y-\gamma\exp(t)\Phi(Qy-u)+\dot{u}. \quad (2.12)$$

The ith-neural dynamic equation of Equation (2.12) can be written as

$$\dot{y}_i = \sum_{j=1}^{n+m}(\delta_{ij}-q_{ij})\dot{y}_j - \sum_{j=1}^{n+m}\dot{q}_{ij}y_j-\gamma\exp(t)\phi\left(\sum_{j=1}^{n+m}q_{ij}y_j-u_i\right)+\dot{u}_i, \quad (2.13)$$

where q_{ij} denotes the ith-row and jth-column element of Q and δ_{ij} denotes the ith-row and jth-column element of identity matrix I. The structure of VP-CDNN is shown in Fig.1.

If the time-varying parameter $\gamma\exp(t)$ is replaced with a constant γ in Equation (2.10), i.e.,

$$\frac{d\varepsilon(t)}{dt} = -\gamma\Phi(\varepsilon(t)) \quad (2.14)$$

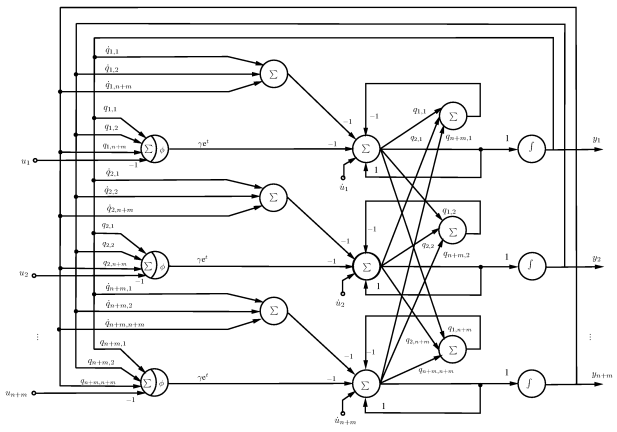

FIGURE 1. Structure of the proposed VP-CDNN.

a fixed-parameter convergent-differential neural network (FP-CDNN) can be obtained by substituting Equation (2.9) into Equation (2.14), i.e.,

$$Q\dot{y} = -\dot{Q}y - \gamma\,\Phi(Qy - u) + \dot{u}. \tag{2.15}$$

III. ROBUSTNESS ANALYSIS

In practical applications, external disturbance and hardware implementation errors always exist when a robot manipulator executes an end-effector tracking task. The roundoff errors in digital computation or electric implementation process may result in these errors or disturbance. Mathematically, a perturbed VP-CDNN model is described as

$$Q\dot{y} = -(\dot{Q} + \Delta D(t))y - \gamma\exp(t)\Phi(Qy - u) + \dot{u} + \Delta s(t) \tag{3.1}$$

where $\Delta D(t) \in R^{(n+m)\times(n+m)}$ denotes differential errors of matrix Q and $\Delta s(t) \in R^{(n+m)}$ denotes differential errors of vector u as well as external disturbance. In the same way, the perturbed FP-CDNN model can be described as

$$Q\dot{y} = -(\dot{Q} + \Delta D(t))y - \gamma\,\Phi(Qy - u) + \dot{u} + \Delta s(t). \tag{3.2}$$

For the perturbed VP-CDNN model (3.1), we have the following theorem on robustness.

Theorem 1: Consider the bounded errors, i.e., $\|\Delta D(t)\|_{\mathrm{F}} \leqslant \theta_D \in R$ and $\|\Delta s(t)\|_2 \leqslant \theta_s \in R$, as well as $\|Q^{-1}\|_{\mathrm{F}} \leqslant \eta_Q \in R$, $\|u\|_2 \leqslant \eta_u \in R$, where $0 \leqslant \theta_D, \theta_s, \eta_Q, \eta_u < +\infty$ with $\|\cdot\|_{\mathrm{F}}$ and $\|\cdot\|_2$ respectively denoting the Frobenius norm of a matrix and the Euclidean norm of a vector, the residual error $\varepsilon(t) = Qy - u$ of the perturbed VP-CDNN model (3.1) using a linear activation-function converges to zero as $t \to +\infty$ and the state variable $y(t)$, starting from any initial state $y(0)$, will converge to the unique theoretical solution $y^*(t)$.

Proof: Since the residual error is defined as $\varepsilon(t) = Qy - u$ in Equation (2.9), the following two equations hold true,

$$y = Q^{-1}(\varepsilon(t) + u) \tag{3.3}$$

$$\dot{\varepsilon}(t) = \dot{Q}y + Q\dot{y} - \dot{u}. \tag{3.4}$$

Substituting Equation (2.9), (3.3), and (3.4) into Equation (3.1), we can get

$$\begin{aligned}\dot{\varepsilon}(t) = &-\gamma\exp(t)\Phi(\varepsilon(t)) - \Delta D(t)Q^{-1}\varepsilon(t)\\ &- \Delta D(t)Q^{-1}u + \Delta s(t).\end{aligned} \tag{3.5}$$

A Lyapunov function candidate is defined as

$$V(t) = \frac{\|\varepsilon(t)\|_2^2}{2} = \frac{\varepsilon^{\mathrm{T}}(t)\varepsilon(t)}{2}. \tag{3.6}$$

Evidently, $V(t)$ is positive definite because $V(t) > 0$ when $\varepsilon(t) \neq 0$, and $V(t) = 0$ if and only if $\varepsilon(t) = 0$. Then consider the time derivative of $V(t)$ in Equation (3.6), i.e.,

$$\begin{aligned}\dot{V}(t) &= \varepsilon^{\mathrm{T}}(t)\Big(-\gamma\exp(t)\Phi(\varepsilon(t)) - \Delta D(t)Q^{-1}\varepsilon(t)\\ &\quad - \Delta D(t)Q^{-1}u + \Delta s(t)\Big)\\ &= -\gamma\exp(t)\varepsilon^{\mathrm{T}}(t)\Phi(\varepsilon(t)) + \varepsilon^{\mathrm{T}}(t)\Delta D(t)Q^{-1}\varepsilon(t)\\ &\quad - \varepsilon^{\mathrm{T}}(t)\Delta D(t)Q^{-1}u + \varepsilon^{\mathrm{T}}(t)\Delta s(t).\end{aligned} \tag{3.7}$$

Since the linear activation-function is employed in the perturbed VP-CDNN model (3.1), the first term of the right side of Equation (3.7) can be rewritten as

$$\begin{aligned}-\gamma\exp(t)\varepsilon^{\mathrm{T}}(t)\Phi(\varepsilon(t)) &= -\gamma\exp(t)\varepsilon^{\mathrm{T}}(t)\varepsilon(t)\\ &= -\gamma\exp(t)\sum_{i=1}^{n+m}\varepsilon_i^2(t).\end{aligned} \tag{3.8}$$

For the second term of the right side of Equation (3.7), it follows from $|\lambda_{\max}(\cdot)| \leqslant \|\cdot\|_{\mathrm{F}}$ [24] that

$$\begin{aligned}\varepsilon^{\mathrm{T}}(t)\Delta D(t)Q^{-1}\varepsilon(t) &\leqslant \varepsilon^{\mathrm{T}}(t)\varepsilon(t)\left|\lambda_{\max}\left(\Delta D(t)Q^{-1}\right)\right|\\ &= \varepsilon^{\mathrm{T}}(t)\varepsilon(t)\left|\lambda_{\max}\left(\Delta D(t)Q^{-1}\right)\right|\\ &\leqslant \varepsilon^{\mathrm{T}}(t)\varepsilon(t)\|\Delta D(t)Q^{-1}\|_{\mathrm{F}}\\ &\leqslant \varepsilon^{\mathrm{T}}(t)\varepsilon(t)\|\Delta D(t)\|_{\mathrm{F}}\|Q^{-1}\|_{\mathrm{F}}\\ &\leqslant \varepsilon^{\mathrm{T}}(t)\varepsilon(t)\theta_D\eta_Q\\ &= \sum_{i=1}^{n+m}\varepsilon_i^2(t)\theta_D\eta_Q.\end{aligned} \tag{3.9}$$

For the third term of the right side of Equation (3.7), it follows $\|A\alpha\|_2 \leqslant \|A\|_{\mathrm{F}}\|\alpha\|_2$ (where A is a matrix and α is a vector) that

$$\begin{aligned}&\varepsilon^{\mathrm{T}}(t)(-\Delta D(t)Q^{-1}u)\\ &\quad\leqslant \sum_{i=1}^{n+m}|\varepsilon_i(t)|\max_{1\leqslant i\leqslant n+m}\left|\left[\Delta D(t)Q^{-1}u\right]_i\right|\\ &\quad\leqslant \sum_{i=1}^{n+m}|\varepsilon_i(t)|\cdot\|\Delta D(t)Q^{-1}u\|_2\\ &\quad\leqslant \sum_{i=1}^{n+m}|\varepsilon_i(t)|\cdot\|\Delta D(t)Q^{-1}\|_{\mathrm{F}}\|u\|_2\\ &\quad\leqslant \sum_{i=1}^{n+m}|\varepsilon_i(t)|\cdot\|\Delta D(t)\|_{\mathrm{F}}\|Q^{-1}\|_{\mathrm{F}}\|u\|_2\\ &\quad\leqslant \sum_{i=1}^{n+m}|\varepsilon_i(t)|\theta_D\eta_Q\eta_u.\end{aligned} \tag{3.10}$$

Similarly, for the forth term of the right side of Equation (3.7), the following inequality holds true, i.e.,

$$\begin{aligned}\varepsilon^{\mathrm{T}}(t)\Delta s(t) &\leqslant \sum_{i=1}^{n+m}|\varepsilon_i(t)|\max_{1\leqslant i\leqslant n+m}|\Delta s_i| \\ &\leqslant \sum_{i=1}^{n+m}|\varepsilon_i(t)|\cdot\|\Delta s\|_2 \\ &\leqslant \sum_{i=1}^{n+m}|\varepsilon_i(t)|\theta_s. \end{aligned} \tag{3.11}$$

Substituting Inequalities (3.8), (3.9), (3.10) and (3.11) into Equation (3.7), we get

$$\begin{aligned}\dot{V}(t) &\leqslant -\gamma\exp(t)\sum_{i=1}^{n+m}\varepsilon_i^2(t)+\sum_{i=1}^{n+m}\varepsilon_i^2(t)\theta_D\eta_Q \\ &\quad+\sum_{i=1}^{n+m}|\varepsilon_i(t)|\theta_D\eta_Q\eta_u+\sum_{i=1}^{n+m}|\varepsilon_i(t)|\theta_s \\ &= -\sum_{i=1}^{n+m}|\varepsilon_i(t)|\Big((\gamma\exp(t)|\varepsilon_i(t)|-\theta_D\eta_Q|\varepsilon_i(t)| \\ &\quad-\theta_D\eta_Q\eta_u-\theta_s\Big)\end{aligned} \tag{3.12}$$

For further discussion, we define

$$\begin{aligned}U(t) &= \gamma\exp(t)|\varepsilon_i(t)|-\theta_D\eta_Q|\varepsilon_i(t)|-\theta_D\eta_Q\eta_u-\theta_s \\ &= (\gamma\exp(t)-\theta_D\eta_Q)(|\varepsilon_i(t)|-\frac{\theta_D\eta_Q\eta_u+\theta_s}{\gamma\exp(t)-\theta_D\eta_Q}).\end{aligned} \tag{3.13}$$

We consider the situation $\gamma\exp(t)-\theta_D\eta_Q > 0$ which can be guaranteed by setting $\gamma > \max(\theta_D\eta_Q/\exp(t))$ since $\exp(t) > 1$. Therefore, Inequation (3.12) can be rewritten as

$$\dot{V}(t) \leqslant -\sum_{i=1}^{n+m}|\varepsilon_i(t)|U(t). \tag{3.14}$$

Evidently, the following three situations should be discussed according to $U(t)$.

1) If $U(t) > 0, \forall i \in \{1, 2, \cdots, n+m\}$, since $|\varepsilon_i(t)| \gtrsim 0$, then $\dot{V}(t) < 0$. According to Lyapunov theorem, considering Lyapunov function $V(t) > 0$ and $\dot{V}(t) < 0$, the dynamic system will tend to be stable, and the error vector $\varepsilon(t)$ will converge to zero gradually and the corresponding state vector $y(t)$ in Equation (2.8) will converge to the optimal solution $y^*(t)$.
2) If $U(t) = 0, \exists i \in \{1, 2, \cdots, n+m\}$, due to $\gamma\exp(t) - \theta_D\eta_Q > 0$, we have $|\varepsilon_i(t)| - (\theta_D\eta_Q\eta_u+\theta_s)/(\gamma\exp(t) - \theta_D\eta_Q) = 0$. We consider in a short enough time period $[t, t+t_0]$, there exists an any small positive value ϵ, which allows $|\varepsilon_i(t+t_0)| - |\varepsilon_i(t+t_0)| < \epsilon$ to hold true. In addition, during $[t, t+t_0]$, $\gamma\exp(t)$ will exponentially increase, then $(\theta_D\eta_Q\eta_u+\theta_s)/(\gamma\exp(t) - \theta_D\eta_Q)$ will decrease, and $U(t) > 0$ again. According to the analysis of case 1), Lyapunov function $V(t) > 0$ and $\dot{V}(t) < 0$, $\varepsilon(t)$ will converge to zero and $y(t)$ will converge to $y^*(t)$.
3) If $U(t) < 0$, i.e., $|\varepsilon_i(t)| < (\theta_D\eta_Q\eta_u+\theta_s)/(\gamma\exp(t) - \theta_D\eta_Q)$, then $-\sum_{i=1}^{n+m}|\varepsilon_i(t)|U(t) > 0$. That is to say, the right hand of Inequality (3.14) is a positive number, and we cannot directly use the Lyapunov theorem. For the sake of discussion, we set $\Delta = -\sum_{i=1}^{n+m}|\varepsilon_i(t)|U(t) > 0$, and Inequality (3.14) is written as $\dot{V}(t) \leqslant \Delta$ with $\Delta > 0$. Two situations can be discussed as bellow.
   a) If $\dot{V}(t) \leqslant 0$ for any time instant, then according to the analysis of case 1) and 2) and Lyapunov theorem, $\varepsilon(t)$ will converge to zero and $y(t)$ will converge to $y^*(t)$.
   b) If $0 < \dot{V}(t) < \Delta$, then $V(t)$ will increase and $\varepsilon(t)$ will diverge outward as time evolves until $|\varepsilon_i(t)| > (\theta_D\eta_Q\eta_u+\theta_s)/(\gamma\exp(t) - \theta_D\eta_Q)$. At that time, $U(t) > 0$ again, and according to the analysis in situation 1) , $\varepsilon(t)$ will converge to zero and $y(t)$ will converge to $y^*(t)$.

Thus the proof is completed. ■

IV. EXPERIMENT VERIFICATION

In this section, two tracking experiments (i.e., butterfly-path tracking task and cardioid-path tracking task) are conducted to verify the effectiveness of the HL-JDF scheme (2.5)-(2.6) synthesized by the VP-CDNN (2.11) on Kinova Jaco^2 manipulator (a six-DOF robot). The task execution period is set as $T = 8$s. The coefficient μ in joint-drift-free criterion (2.5) is set as $\mu = 4$. Parameters $\alpha, \beta, \rho_v, \rho_p = 20$. The feedback-control matrix K is set as an identity matrix. The initial state is $\theta(0) = [1.68; 2.81; -3.22; 4.19; -1.71; -2.65]$ rad.

A. EXPERIMENT VERIFICATION OF THE HL-JDF SCHEME

In this subsection, comparison simulations between the conventional MTN scheme (i.e., $\zeta = 0$) and the proposed HL-JDF scheme ($\zeta = 0.6$ in this simulation) are presented. Both the MTN scheme and HL-JDF scheme are synthesized by the conventional FP-CDNN (2.15). The simulation results are analyzed in terms of the joint-state, joint-velocity, joint-acceleration and joint-torque. For butterfly-path tracking task, the corresponding results are illustrated in Fig. 2. Specifically, Figs. 2(a), (c), (e) and (g) are the simulation results of the conventional MTN scheme. Figs. 2(b), (d), (f) and (h) are the simulation results of the proposed HL-JDF scheme.

Firstly, as can be seen from Fig. 2(a), the final state of the manipulator does not return to its initial state when finishing a cyclic motion. That is to say, there exits obvious joint-drift phenomenon of the manipulator in the closed butterfly-path tracking task of the conventional MTN scheme, and this should be evitable in repetitive industrial process. On the contrary, as illustrated in Fig. 2(b), the final state of the manipulator coincides well with its final state the butterfly-path tracking task is synthesized by the proposed HL-JDF scheme.

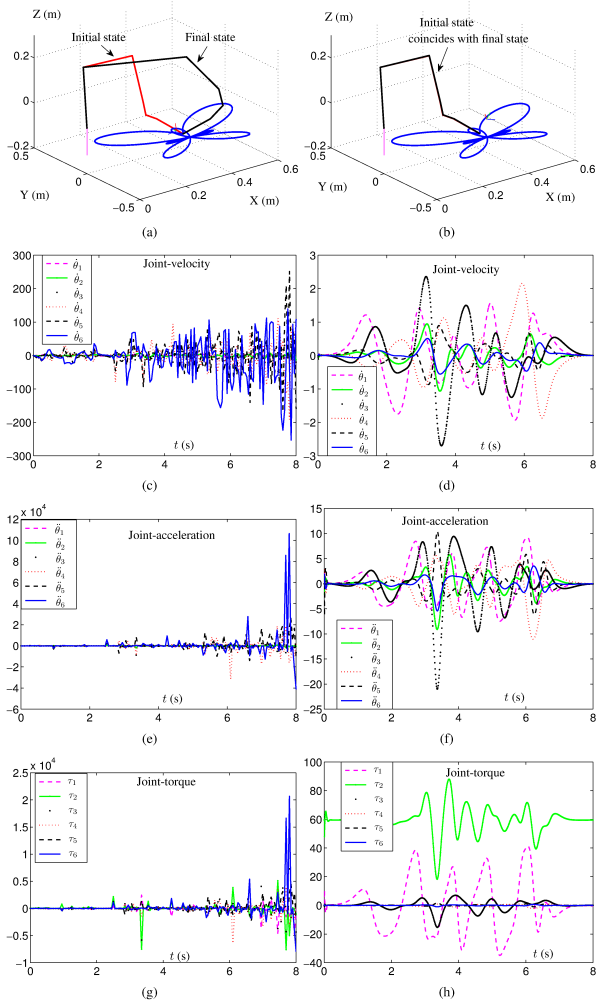

FIGURE 2. Comparison simulations between MTN scheme and HL-JDF scheme in butterfly-path tracking task. (a) Joint space of MTN scheme. (b) Joint space of HL-JDF scheme. (c) Joint-velocity of MTN scheme. (d) Joint-velocity of HL-JDF scheme. (e) Joint-acceleration of MTN scheme. (f) Joint-acceleration of HL-JDF scheme.

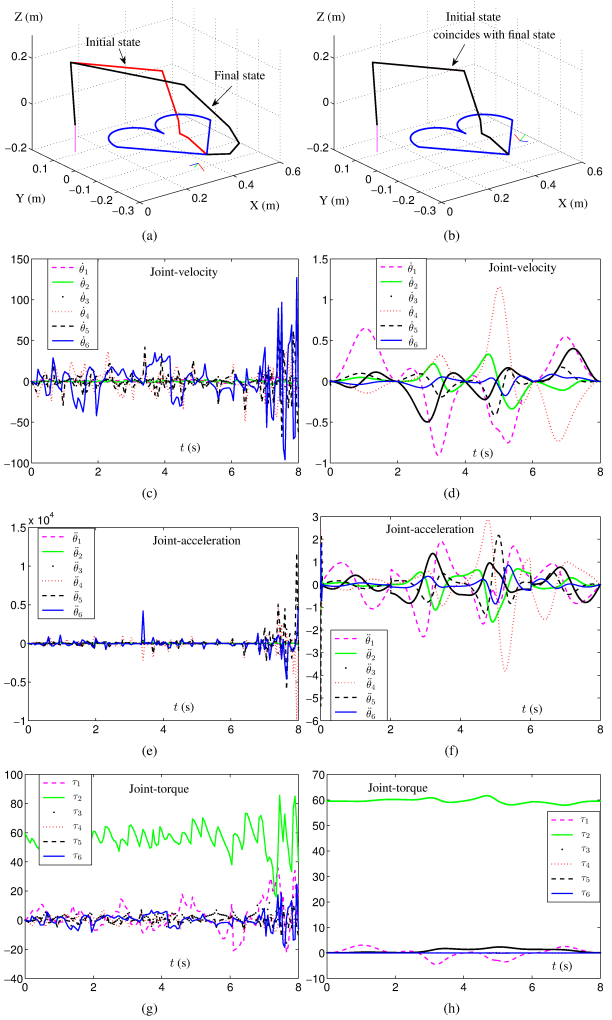

FIGURE 3. Comparison simulations between MTN scheme and HL-JDF scheme in cardioid-path tracking task. (a) Joint space of MTN scheme. (b) Joint space of HL-JDF scheme. (c) Joint-velocity of MTN scheme. (d) Joint-velocity of HL-JDF scheme. (e) Joint-acceleration of MTN scheme. (f) Joint-acceleration of HL-JDF scheme.

Secondly, there exist extremely high joint-velocity, joint-acceleration and joint-torque and divergence problem during the butterfly-path tracking task execution period of the MTN scheme, which are illustrated in Figs. 2(c), (e) and (g), respectively. This is impossible and dangerous in actual implementing process. Nevertheless, as can be seen from Figs. 2(d), (f) and (h) the HL-JDF scheme can effectively prevent the divergence and oscillation of joint-velocity, joint-acceleration and joint-torque.

Moreover, in order to further demonstrate the widely applicability of the proposed HL-JDF scheme, another closed tracking task (i.e. cardioid-path tracking task) is also conducted. The similar simulation results can be obtained from Fig. 3. Large joint-drift exists in the cardioid-path tracking task of the conventional MTN scheme (as shown in Fig. 3(a)). By contrast, as can been seen from Fig. 3(b), the final state of the manipulator coincides well with the initial state in the tracing task of the HL-JDF scheme. That is a joint-drift-free cyclic motion. Similarly, the divergence and oscillation problems are obvious in the tracking task of the MTN scheme (as shown in Figs. 3(d), (f), and (h)). On the contrary, illustrated in Figs. 3(c), (e), and (g), the smooth and acceptable joint-velocity, joint-acceleration, and joint-torque can be obtained in the tracking task of the HL-JDF scheme.

In summary, the comparison simulation results can demonstrate the effectiveness of the proposed HL-JDF scheme for solving inverse-kinematics problem of redundant robot manipulators. In addition, compared with the conventional MTN scheme, the proposed HL-JDF scheme can remedy the joint-drift problem of redundant robot manipulators in cyclic tracking tasks, and the divergence of joint-velocity, joint-acceleration, and joint-torque can be prevented.

B. EXPERIMENT VERIFICATION OF THE VP-CDNN MODEL

In actual applications, when robot manipulators are executing tasks, the hardware implementation, external disturbances and digital computation errors always exist. In this subsection, in order to demonstrate the robustness of the proposed

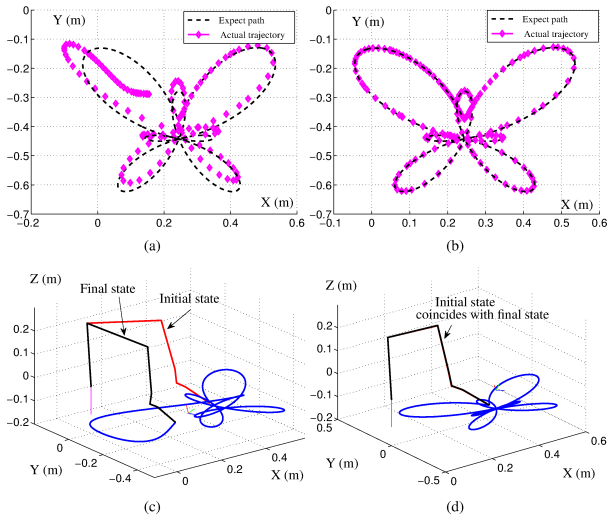

FIGURE 4. Computer simulations of butterfly-path tracking task of the HL-JDF scheme synthesized by FP-CDNN and VP-CDNN. (a) Tracking trajectories synthesized by FP-CDNN for butterfly-path tracking task. (b) Tracking trajectories synthesized by VP-CDNN for butterfly-path tracking task. (c) Joints space of butterfly-path synthesized by FP-CDNN. (d) Joints space of butterfly-path synthesized by VP-CDNN.

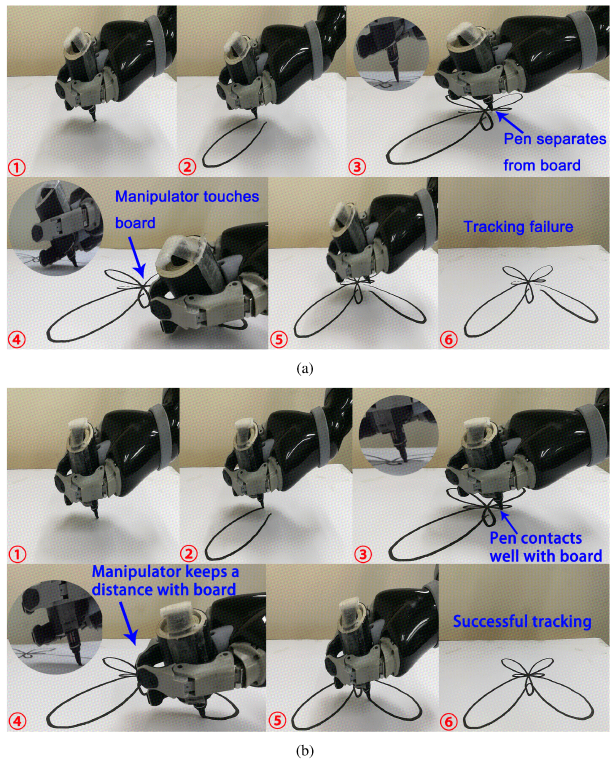

FIGURE 5. Physical experiments of butterfly-path tracking task of the HL-JDF scheme synthesized by FP-CDNN and VP-CDNN performed on the Kinova JACO^2 robot manipulator. (a) Snapshots of butterfly-path tracking task synthesized by FP-CDNN. (b) Snapshots of butterfly-path tracking task synthesized by VP-CDNN.

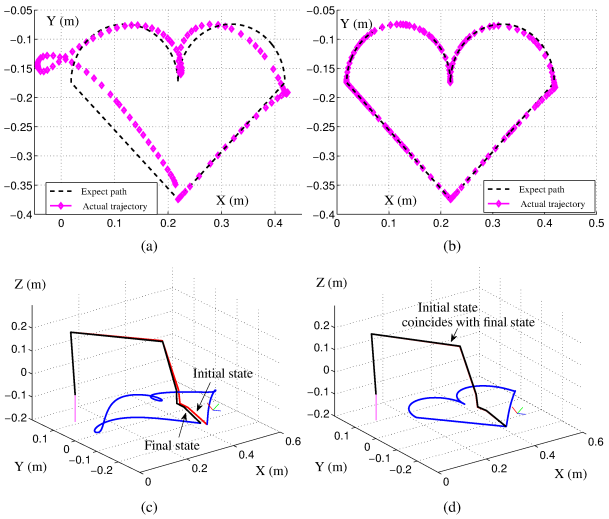

FIGURE 6. Computer simulations of cardioid-path tracking task of the HL-JDF scheme synthesized by FP-CDNN and VP-CDNN. (a) Tracking trajectories synthesized by FP-CDNN for cardioid-path tracking task. (b) Tracking trajectories synthesized by VP-CDNN for cardioid-path tracking task. (c) Joints space of cardioid-path synthesized by FP-CDNN. (d) Joints space of cardioid-path synthesized by VP-CDNN.

VP-CDNN, comparison experiments between the conventional perturbed FP-CDNN model (3.2) and the proposed perturbed VP-CDNN model (3.1) are conducted, and the external perturbation and digital computation errors in Equations (3.2) and (3.1) are depicted as sine or cosine functions. The conventional FP-CDNN and the proposed VP-CDNN are exploited to solve the HL-JDF scheme where parameters are set as $\zeta = 0.8$, $\rho_{\mathrm{v}} = \rho_{\mathrm{p}} = 20$, $\alpha = \beta = 50$, and $\gamma = 200$.

Firstly, the tracking trajectory of the butterfly-path synthesized by FP-CDNN and VP-CDNN are shown in Figs. 4 (a) and (b), respectively. Obviously, there exits large error between the tracking trajectory synthesized by FP-CDNN and the expected path (as shown in Fig. 4 (a)), and joint-drift phenomenon happens because the robot manipulator does not return to its initial state when finishing a cyclic motion (as shown in Fig. 4 (c)). By contrast, the trajectory synthesized by VP-CDNN can fit well with the expected path (as shown in Fig. 4 (b)). Meanwhile, the final state of manipulator coincides well with the initial state (as shown in Fig. 4 (d). The snapshots of physical experiments are illustrated in Fig. 5. As shown in Fig. 5(a), the butterfly-path tracking task synthesized by FP-CDNN fails due to large position errors. Specifically, due to large errors, the pen fixed on the end-effector cannot continue writing on the board, which can be seen from snapshot 3 of Fig. 5(a) and the manipulator collides with the drawing board as shown in snapshot 4 of Fig. 5(a). Evidently, the tracking task failed. It is worth pointing out this experiment is a bit dangerous since the robot manipulator may be damaged. However, the butterfly-path tracking task synthesized by VP-CDNN is finished very well as shown in Fig. 5(b). Because of the strong disturbance-resistant performance of VP-CDNN, the pen always works well on the drawing board as shown in snapshot 3 of Fig. 5(b) and the manipulator can keep

a constant distance with the drawing board as shown in snapshot 4 of Fig. 5(b).

Secondly, similar to the butterfly-path tracking task, the simulation results can be obtained in the cardioid-path tracking task. The cardioid-path tracking task synthesized by FP-CDNN cannot be finished well with perturbation considered. Specially, there exists large errors between the actual trajectory and expected cardioid-path as shown in Fig. 6(a) and the final state cannot return to the initial state of redundant robot manipulators as shown in Fig. 6(c). However, the trajectory synthesized by the VP-CDNN can fit well with the expected path as shown in Fig. 6(b) and a repetitive motion is finished as shown in Fig. 6(d). The physical experiments of cardioid-path tracking task can further demonstrate the effectiveness and robustness of the proposed VP-CDNN to finish the cardioid-path tracking task (see Fig. 7).

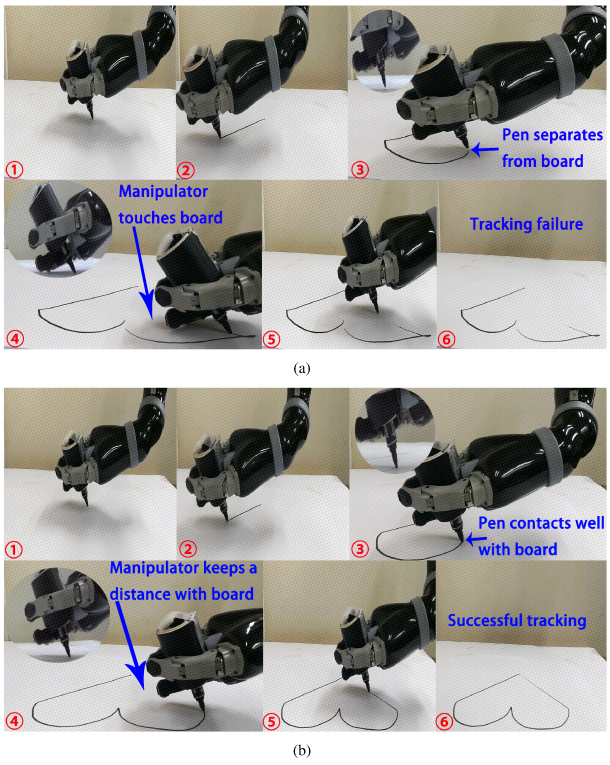

FIGURE 7. Physical experiments of cardioid-path tracking task of the HL-JDF scheme synthesized by FP-CDNN and VP-CDNN performed on the Kinova JACO^2 robot manipulator. (a) Snapshots of cardioid-path tracking task synthesized by FP-CDNN. (b) Snapshots of cardioid-path tracking task synthesized by VP-CDNN.

In summary, the above two experiments further illustrate the robustness of the VP-CDNN for solving the perturbed tracking problem of redundant robot manipulators.

V. CONCLUSIONS

In this paper, a hybrid-level joint-drift-free (HL-JDF) scheme is developed and investigated to remedy the joint-drift problem of redundant robot manipulators in cyclic motion process. The proposed HL-JDF scheme can also prevent high joint-velocity, joint-acceleration and joint-torque. Meanwhile, the divergence and vibration problems can be resisted. Moreover, a novel varying-parameter convergent-differential neural network (VP-CDNN) is proposed to solve the HL-JDF scheme. Due to the super exponential convergence rate, the proposed VP-CDNN is robustness and with inherent perturbation tolerance. Comparison simulations and experiments verify the effectiveness of the HL-JDF scheme and robustness of the VP-CDNN for solving the inverse-kinematics problem of redundant robot manipulators. The future work is to integrate the fuzzy control and self-adaption control with the proposed neural network model.

REFERENCES

[1] T. Morita, K. Mase, Y. Hirano, and S. Kajita, "Reciprocal attentive communication in remote meeting with a humanoid robot," in *Proc. Int. Conf. Multimodal Interfaces*, Nov. 2007, pp. 228–235.
[2] M. Elbanhawi and M. Simic, "Sampling-based robot motion planning: A review," *IEEE Access*, vol. 2, pp. 56–77, 2014.
[3] C. Yang, X. Wang, L. Cheng, and H. Ma, "Neural-learning-based telerobot control with guaranteed performance," *IEEE Trans. Cybern.*, vol. 47, no. 10, pp. 3148–3159, Oct. 2017.
[4] B. Whitsell and P. Artemiadis, "Physical human–robot interaction (pHRI) in 6 DOF with asymmetric cooperation," *IEEE Access*, vol. 5, no. 99, pp. 10834–10845, 2017.
[5] K. Ito and M. Iwasaki, "State feedback-based vibration suppression for multi-axis industrial robot with posture change," in *Proc. Annu. Conf. IEEE Ind. Electron. Soc. (IECON)*, Oct. 2016, pp. 5119–5124.
[6] H. Cervantes-Culebro, C. A. Cruz-Villar, M. G. M. Peñaloza, and E. Mezura-Montes, "Constraint-handling techniques for the concurrent design of a five-bar parallel robot," *IEEE Access*, vol. 5, pp. 23010–23021, 2017.
[7] D. Guo, and K. Li, "Acceleration-level obstacle-avoidance scheme for motion planning of redundant robot manipulators," in *Proc. IEEE Int. Conf. Robot. Biomimetics*, Dec. 2017, pp. 1313–1318.
[8] M. Jin, C. Zhou, and Y. Liu, "Hybrid impedance control of 7-DOF redundant manipulator with dual compliant surface," *IEEE Int. Conf. Mechatronics Automat*, Aug. 2015, pp. 1424–1429.
[9] J. Long, L. Shuai, H. M. La, and X. Luo, "Manipulability optimization of redundant manipulators using dynamic neural networks," *IEEE Trans. Ind. Electron.*, vol. 64, no. 6, pp. 4710–4720, Jun. 2017.
[10] W. Xu, J. Zhang, B. Liang, and B. Li, "Singularity analysis and avoidance for robot manipulators with nonspherical wrists," *IEEE Trans. Ind. Electron.*, vol. 63, no. 1, pp. 277–290, Jan. 2016.
[11] K. Chen, L. Zhang, and Y. Zhang, "Cyclic motion generation of multi-link planar robot performing square end-effector trajectory analyzed via gradient-descent and Zhang et al's neural-dynamic methods," in *Proc. Int. Symp. Syst. Control Aerosp. Astronaut.*, Dec. 2008, pp. 1–6.
[12] Z. Zhang, L. Zheng, J. Yu, Y. Li, and Z. Yu, "Three recurrent neural networks and three numerical methods for solving a repetitive motion planning scheme of redundant robot manipulators," *IEEE/ASME Trans. Mechantron.*, vol. 22, no. 3, pp. 1423–1434, Jun. 2017.
[13] C. A. Klein, and C. H. Huang, "Review of pseudoinverse control for use with kinematically redundant manipulators," *IEEE Trans. Syst., Man, Cybern. Syst.*, vol. SMC-13, no. 2, pp. 245–250, Mar./Apr. 1983.
[14] D. Guo and Y. Zhang, "Different-level two-norm and infinity-norm minimization to remedy joint-torque instability/divergence for redundant robot manipulators," *Robot. Auto. Syst.*, vol. 60, no. 6, pp. 874–888, 2012.
[15] Y. Zhang, D. Guo, and S. Ma, "Different-level simultaneous minimization of joint-velocity and joint-torque for redundant robot manipulators," *J. Intell. Robot. Syst.*, vol. 72, no. 3, pp. 301–323, 2013.
[16] Y.-J. Chen, M.-Y. Ju, and K.-S. Hwang, "A virtual torque-based approach to kinematic control of redundant manipulators," *IEEE Trans. Ind. Electron.*, vol. 64, no. 2, pp. 1728–1736, Feb. 2017.
[17] Y. Zhang, S. S. Ge, and T. H. Lee, "A unified quadratic-programming-based dynamical system approach to joint torque optimization of physically constrained redundant manipulators," *IEEE Trans. Syst., Man, Cybern. B, Cybern.*, vol. 34, no. 5, pp. 2126–2132, Oct. 2004.

[18] Y. Xia, "A new neural network for solving linear programming problems and its application," *IEEE Trans. Neural Netw.*, vol. 7, no. 2, pp. 525–529, Mar. 1996.
[19] J. Wang, Q. Hu, and D. Jiang, "A Lagrangian network for kinematic control of redundant robot manipulators," *IEEE Trans. Neural Netw.*, vol. 10, no. 5, pp. 1123–1132, Sep. 1999.
[20] S. Li, J. He, Y. Li, and M. U. Rafique, "Distributed recurrent neural networks for cooperative control of manipulators: A game-theoretic perspective," *IEEE Trans. Neural Netw. Learn. Syst.*, vol. 28, no. 2, pp. 415–426, Feb. 2017.
[21] L. Jin, Y. Zhang, S. Li, and Y. Zhang, "Modified ZNN for time-varying quadratic programming with inherent tolerance to noises and its application to kinematic redundancy resolution of robot manipulators," *IEEE Trans. Ind. Electron.*, vol. 63, no. 11, pp. 6978–6988, Nov. 2016.
[22] J. Wang, "Recurrent neural network for solving quadratic programming problems with equality constraints," *Electron. Lett.*, vol. 28, no. 14, pp. 1345–1347, Jul. 1992.
[23] Y. Zhang, D. Jiang, and J. Wang, "A recurrent neural network for solving Sylvester equation with time-varying coefficients," *IEEE Trans. Neural Netw.*, vol. 13, no. 5, pp. 1053–1063, Sep. 2002.
[24] Y. Zhang, G. Ruan, K. Li, and Y. Yang, "Robustness analysis of the Zhang neural network for online time-varying quadratic optimization," *J. Phys. A, Math. Theor.*, vol. 43, no. 24, p. 245202, 2010.
[25] Z.-J. Zhang and Y.-N. Zhang, "Equivalence of different-level schemes for repetitive motion planning of redundant robots," *Acta Autom. Sin.*, vol. 39, no. 1, pp. 88–91, Jan. 2013.

ZHIJUN ZHANG (M'12) received the Ph.D. degree in communication and information system from Sun Yat-sen University, Guangzhou, China, in 2012. He was a Post-Doctoral Research Fellow with the Institute for Media Innovation, Nanyang Technological University, Singapore, from 2013 to 2015. Since 2015, he has been an Associate Professor with the School of Automation Science and Engineering, South China University of Technology, Guangzhou, China. His current research interests include robotics, neural networks, and human–robot interaction.

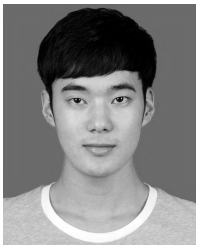

ZIYI YAN received the B.E. degree in automation from Central South University, Changsha, China, in 2016. He is currently pursuing the M.S. degree at the School of Automation Science and Engineering, South China University of Technology, Guangzhou, China. His current research interests include robotics, neural networks, and machine learning.